Buckling Analysis of Geometrically Imperfect Stiffened Cylinders under Axial Compression

Izhak Sheinman* and George J. Simitses†
Georgia Institute of Technology, Atlanta, Ga.

The buckling analysis of an imperfect, thin, circular, cylindrical, stiffened shell under uniform axial compression and for various end conditions is investigated. A methodology is presented for predicting critical conditions for such configurations. This methodology is based on the smeared technique and the von Karman-Donnell nonlinear kinematic relations in the presence of geometric imperfections. The computational procedure employs a Fourier series type of separated solution, and through the Galerkin procedure the field equations are reduced to a system of ordinary differential equations. These equations are solved by the finite-difference scheme. Numerical results for numerous stiffened and unstiffened configurations are presented.

Nomenclature

A	= area
A_x, A_y	= stringer and ring cross-sectional area
D	= flexural stiffness of the skin
E	= Young moduli of elasticity
E_{xx}	= extensional stiffness of the skin
e_x, e_y	= stringer and ring eccentricities (positive inward)
e	= unit end shortening
F	= stress function
f_i	= Fourier coefficient of stress function
I_{xc}, I_{yc}	= stringer and ring moment of inertia about their centroidal axes
K	= number of terms in truncated Fourier series
ℓ_x, ℓ_y	= stringer and ring spacings
ℓ	= mesh point
L	= total length of the shell
M_{xx}, M_{yy}, M_{xy}	= moment resultants
m	= number of axial half waves
N_{xx}, N_{yy}, N_{xy}	= stress resultants
$\bar{N}_{xx}$	= applied compressive load
N_{xcl}	= classical buckling load
N_{xcr}	= critical load (limit point)
n	= number of circumferential full waves
NP	= number of points in axial direction
Q^*	= effective transverse shear
R	= radius of the cylinder
t	= skin thickness
U_T	= total potential
u, v	= in-plane displacements
w	= radial displacement (positive inward)
w°	= radial geometric imperfection
x, y, z	= coordinate system
Z	= Batdorf curvature parameter $[=L^2(1-\nu^2)^{1/2}/R\cdot t]$
z	= unknowns vector
$\epsilon_{xx}, \epsilon_{yy}, \epsilon_{xy}$	= reference surface strains
$\kappa_{xx}, \kappa_{yy}, \kappa_{xy}$	= reference surface changes in curvature and torsion
$\lambda_{xx}, \lambda_{yy}$	= smeared extensional stiffnesses of stringers and rings
ρ_{xx}, ρ_{yy}	= smeared flexural stiffnesses of stringers and rings
ν	= Poisson's ratio
Δ	= interval size between mesh point
$(\,)' = [\,], x$	= derivative with respect to x

Received April 6, 1975; revision received Nov. 1, 1976.
Index categories: Structural Stability Analysis; Structural Static Analysis.

*Posdoctoral Fellow, School of Engineering Science and Mechanics (on leave from Technion-Israel Institute of Technology, Haifa, Israel).
†Professor, School of Engineering Science and Mechanics. Associate Fellow AIAA.

I. Introduction

STABILITY of thin, circular, cylindrical shells (with or without stiffening), because of its importance, has employed tremendous attention for the past seventy years. Although a complete understanding of all the details of the phenomena involved has not yet been reached, it has been well established that the discrepancy between classical theoretical predictions and experimental results lies primarily in the fact that the system is sensitive to geometric imperfection, the presence of which is unavoidable.

The imperfection sensitivity of the system was initially established through strict postbuckling analyses of the perfect geometry system. In addition, it was explained that the load carrying capacity of such systems is directly related to the lowest load corresponding to postbuckling states of equilibrium. The first theoretical investigation of this type was reported by von Kármán and Tsien[1] in 1941. The investigators calculated postbuckling equilibrium states, for an unstiffened, axially compressed, thin, circular, cylindrical shell, corresponding to loads far below the classical critical load. The calculations were based on a number of simplifying assumptions, the most important being the neglect of the effect of the boundary conditions. Many subsequent investigators[2-4] attempted to improve the calculations of von Kármán and Tsien in order to find the smallest postbuckling equilibrium load. This search came to an end when Hoff, Madsen, and Mayers[5] found in their calculations that the minimal postbuckling load tended towards zero with improved functional representation (taking more and more terms in the series) for the solution to the governing equations and with diminishing thickness. In addition, Madsen and Hoff[6] repeated the investigation by employing more accurate kinematic relations than those of Donnell. The difference between these results and the previous ones was insignificant. Furthermore, Koiter[7] has shown that the von Kármán-Donnell equations are also applicable to problems with arbitrarily large displacements, when the function describing the radial displacement is taken to be the curvature function defined in his paper.

Koiter[8] was the first to question the use of the minimal postbuckling equilibrium load as a measure of the load

carrying capacity of the configuration. Instead, he proposes to find the critical load (limit point) of the imperfect system. Koiter's work is the first attempt to analyze the buckling of an imperfect shell, but his method is limited to the neighborhood of the classical load and therefore to small imperfections of certain spatial form. This approach has been adopted by many investigators including Hutchinson and Amazigo[9] who treated the stringer or ring-stiffened, thin, cylindirical shell. Excellent reviews on the subject may be found in the works of Hoff[10] and Hutchinson and Koiter.[11]

Many of the postbuckling analyses that are based on Koiter's proposition[11] disregard the effect of end conditions by assuming that the cylinder length is extremely large. A systematic experimental investigation dealing with cylinders of various lengths[12] revealed that the postbuckling behavior is strongly influenced by the cylinder length. Narasinham and Hoff[13] analyzed an unstiffened, thin, circular, cylindrical, imperfect shell of finite length under uniform axial compression. They solve the nonlinear equations by employing a separated series solution for the dependent variables, each term of which contained a function of x multiplied by a cosine term in y (Fourier). Thus the equations are reduced to a system of ordinary differential equations, which in turn are solved by the finite-difference scheme. Although the equations are developed for arbitrary terms of Fourier series, the solution is restricted to just one term for the displacement function. A similar procedure, but one that employs the "shooting method"[14] instead of the finite-difference technique, is employed by Arbocz and Sechler[15] in their investigation of the buckling behavior of axially compressed, imperfect, cylindrical shells.

Finally, Ball and his collaborators (see Ref. 16 and the cited references therein) have developed a computer program, SATANS and SATANS-II (Static and Transient Analysis, Nonlinear, Shells) which solves for the static and dynamic response of shells of revolution (with or without imperfections) by step-incrementing the applied load. The nonlinear field equations employed are based on Sander's kinematic relations corresponding to small strains but moderately small rotations.

With the exception of the work of Ref. 9, there is virtually no reported investigation on the buckling behavior of imperfect stiffened configurations. The present paper presents a methodology for analyzing the buckling of a uniformly compressed, stiffened (rings and stringers), thin, circular, cylindrical, imperfect shell of finite length and various boundary conditions. The analysis employs the von Kármán-Donnell large displacement equations and the smeared technique. The solution procedure is similar to that of Ref. 13, but the limitations on the spatial character of the imperfection has been relaxed considerably. Results have been produced for special case geometries that have been reported in the open literature (bench marks) and for new configurations of the stiffened type in both directions.

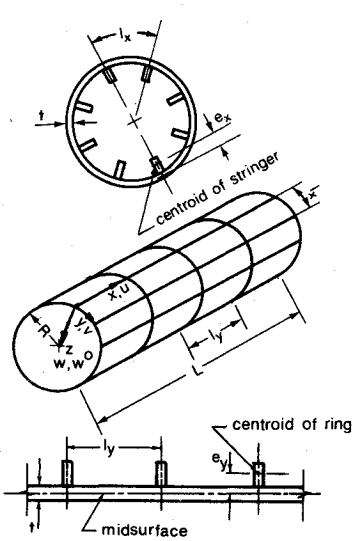

Fig. 1 Geometry and sign convention.

II. Mathematical Formulation

By employing the von Kármán-Donnell kinematic equations for geometrically imperfect $[w^\circ(x,y)]$, thin, cylindrical shells one can easily derive the compatibility and transverse equilibrium equations in terms of the radial displacement w and the stress function F, as well as the expressions for the total potential and the "unit end shortening." The procedure employed is similar to that outlined in Ref. 13 for unstiffened, imperfect, thin, cylindrical shells.

Consider a geometrically imperfect stiffened cylinder under uniform axial compression. Let $w^\circ(x,y)$ denote the deviation of the shell midsurface (taken to be the reference surface) from the corresponding perfectly cylindrical one. Let u,v, and w denote the displacements of material points on the reference surface (Fig. 1).

The kinematic relations, first proposed by Donnell[17] are as follows

$$\epsilon_{xx}=u_{,x}+\tfrac{1}{2}(w_{,x}^2+2w_{,x}w^\circ_{,x}) \tag{1a}$$

$$\epsilon_{yy}=v_{,y}-w/R+\tfrac{1}{2}(w_{,y}^2+2w_{,y}w^\circ_{,y}) \tag{1b}$$

$$\gamma_{xy}=2\epsilon_{xy}=u_{,y}+v_{,x}+w_{,x}w_{,y}+w_{,y}w^\circ_{,x}+w_{,x}w^\circ_{,y} \tag{1c}$$

$$\kappa_{xx}=w_{,xx};\quad \kappa_{yy}=w_{,yy};\quad \kappa_{xy}=w_{,xy} \tag{1d,e,f}$$

The stress and moment resultants to strains and changes in curvature and torsion are taken from Ref. 18. They were derived by employing the smeared technique.

$$N_{xx}=E_{xx_p}[(1+\lambda_{xx})\epsilon_{xx}+\nu\epsilon_{yy}-e_x\lambda_{xx}\kappa_{xx}] \tag{2a}$$

$$N_{yy}=E_{xx_p}[\nu\epsilon_{xx}+(1+\lambda_{yy})\epsilon_{yy}-e_y\lambda_{yy}\kappa_{yy}] \tag{2b}$$

$$N_{xy}=E_{xx_p}[(1-\nu)\epsilon_{xy}] \tag{2c}$$

$$M_{xx}=D\left\{\left[(1+\rho_{xx})+\frac{12}{t^2}e_x^2\lambda_{xx}\right]\kappa_{xx}+\nu\kappa_{yy}-\frac{12}{t^2}e_x\lambda_{xx}\epsilon_{xx}\right\} \tag{2d}$$

$$M_{yy}=D\left\{\nu\kappa_{xx}+\left[(1+\rho_{yy})+\frac{12}{t^2}e_y^2\lambda_{yy}\right]\kappa_{yy}-\frac{12}{t^2}e_y\lambda_{yy}\epsilon_{yy}\right\} \tag{2e}$$

$$M_{xy}=D(1-\nu)\kappa_{xy} \tag{2f}$$

where

$$E_{xx_p}=Et/(1-\nu^2);\qquad D=Et^3/12(1-\nu^2)$$

$$\lambda_{xx}=A_x(1-\nu^2)/t\ell_x;\qquad \lambda_{yy}=A_y(1-\nu^2)/t\ell_y$$

$$\rho_{xx}=EI_{xc}/D\ell_x;\qquad \text{and}\quad \rho_{yy}=EI_{yc}/D\ell_y$$

From Eqs. (2) one may derive the following expressions for the reference surface strains

$$\epsilon_{xx}=a_1N_{xx}+a_2N_{yy}+a_3\kappa_{xx}+a_4\kappa_{yy} \tag{3a}$$

$$\epsilon_{yy}=a_2N_{xx}+b_2N_{yy}+b_3\kappa_{xx}+b_4\kappa_{yy} \tag{3b}$$

$$\epsilon_{xy}=\tfrac{1}{2}\gamma_{xy}=N_{xy}/(1-\nu)E_{xx_p} \tag{3c}$$

where

$$a_1=(1+\lambda_{yy})/\alpha E_{xx_p};\qquad a_2=-\nu/\alpha E_{xx_p};$$

$$a_3=(1+\lambda_{yy})e_x\lambda_{xx}/\alpha;\qquad a_4=-\nu e_y\lambda_{yy}/\alpha;$$

$$b_2=(1+\lambda_{xx})/\alpha E_{xx_p};\qquad b_3=-\nu e_x\lambda_{xx}/\alpha$$

$$b_4=(1+\lambda_{xx})e_y\lambda_{yy}/\alpha;\qquad \alpha=[(1+\lambda_{xx})(1+\lambda_{yy})-\nu^2] \tag{4}$$

By employing the principle of the stationary value of the total potential one can derive the following equilibrium equations

$$N_{xx,x}+N_{xy,y}=0 \tag{5a}$$

$$N_{xy,x}+N_{yy,y}=0 \tag{5b}$$

$$M_{xx,xx}+2M_{xy,xy}+M_{yy,yy}=\frac{N_{yy}}{R}+[N_{yy}(w_{,y}+w^{\circ}_{,y})]_{,y}$$
$$+[N_{xy}(w_{,x}+w^{\circ}_{,x})]_{,y}+[N_{xx}(w_{,x}+w^{\circ}_{,x})]_{,x}$$
$$+[N_{xy}(w_{,y}+w^{\circ}_{,y})]_{,x} \tag{5c}$$

By introducing the Airy stress function, as $N_{xx}=-\bar{N}_{xx}-F_{,yy}, N_{yy}=F_{,xx}$ and $N_{xy}=-F_{,xy}$ where $\bar{N}_{xx}$ is the level of the applied uniform axial compression, the first two of Eqs. (5) are identically satisfied.

Next, by eliminating u and v from the first three of Eqs. (1), employing Eqs. (3), the Airy stress function, and the last three of Eqs. (1) one can derive the compatibility equation in terms of the Airy stress function F_1 and the radial displacement w. If one expresses the third of Eq. (5) in terms of F and w, the governing equations consist of two coupled partial differential equations in F and w. These are

Equilibrium

$$DL_h[w]-L_q[F]-F_{,xx}/R+\bar{N}_{xx}(w_{,xx}+w^{\circ}_{,xx})$$
$$-L[F,w+w^{\circ}]=0 \tag{6}$$

Compatibility

$$L_d[F]+L_q[w]+\tfrac{1}{2}L[w,w+2w^{\circ}]+w_{,xx}/R=0 \tag{7}$$

where L_d, L_h, and L_q are differential operators defined by L_g,

$$L_g[s]=g_{11}s_{,xxxx}+2g_{12}S_{,xxyy}+g_{22}S_{,yyyy} \tag{8a}$$

with

$$d_{11}=(1+\lambda_{xx})/\alpha E_{xx_p}$$
$$d_{12}=[(1+\lambda_{xx})(1+\lambda_{yy})-\nu]/\alpha(1-\nu)E_{xx_p}$$
$$d_{22}=(1+\lambda_{yy})/\alpha E_{xx_p} \tag{9a}$$

$$h_{11}=1+\rho_{xx}+\frac{12}{t^2}\cdot\frac{e_x^2\lambda_{xx}(1+\lambda_{yy}-\nu^2)}{\alpha}$$

$$h_{12}=1+\frac{12}{t^2}\frac{\nu e_x e_y\lambda_{xx}\lambda_{yy}}{\alpha}$$

$$h_{22}=1+\rho_{yy}+\frac{12}{t^2}\frac{e_y^2\lambda_{yy}(1+\lambda_{xx}-\nu^2)}{\alpha} \tag{9b}$$

$$q_{11}=-\nu e_x\lambda_{xx}/\alpha$$

$$q_{12}=[(1+\lambda_{yy})e_x\lambda_{xx}+(1+\lambda_{xx})e_y\lambda_{yy}]/(2\alpha)$$

$$q_{22}=-\nu e_y\lambda_{yy}/\alpha \tag{9c}$$

and L is a differential operator defined by

$$L[S,T]=S_{,xx}T_{,yy}-2S_{,xy}T_{,xy}+S_{,yy}T_{,xx} \tag{8b}$$

The total potential expression, in terms of the Airy stress function and the radial displacement, is as follows

$$U_T=\frac{1}{2E_{xx_p}}\int_A(\beta_1F_{,yy}^2+\beta_2F_{,xx}^2+\beta_3F_{,xx}F_{,yy}+\beta_4F_{,xy}^2)\,dA$$
$$\frac{D}{2}\int_A(\alpha_1w_{,yy}^2+\alpha_2w_{,xx}^2+\alpha_3w_{,xx}w_{,yy}+\alpha_4w_{,xy}^2)\,dA$$
$$-\frac{\bar{N}_{xx}}{2E_{xxp}}\int_A(2\beta_1F_{,yy}+\beta_3F_{,xx})\,dA$$
$$+\frac{\beta_1}{E_{xxp}}\pi RL\,\bar{N}_{xx}^2-\bar{N}_{xx}2\pi RLe_{AV} \tag{10}$$

where e_{AV} (average end shortening) is given by

$$e_{AV}=-\int_A u_{,x}dA/2\pi RL$$

and

$$\beta_1=d_{22}E_{xxp};\quad \beta_2=d_{11}E_{xxp};\quad \beta_3=-2\nu/\alpha;\quad \beta_4=2/(1-\nu)$$

$$\alpha_1=h_{22};\quad \alpha_2=h_{11};\quad \alpha_3=2\nu\left[1+\frac{12}{t^2}\frac{e_xe_y\lambda_{xx}\lambda_{yy}}{\alpha}\right];$$

$$\alpha_4=2(1-\nu) \tag{11}$$

Similarly, the expressions for the average end shortening and "unit end shortening" at $y=0$ are given by

$$e_{AV}=\alpha_1\bar{N}_{xx}-\frac{1}{2\pi RL}\int_0^{2\pi R}\int_0^L[a_1F_{,yy}+a_2F_{,xx}$$
$$+a_3w_{,xx}+a_4w_{,yy}-\frac{1}{2}w_{,x}(w_{,x}+2w^{\circ}_{,x})]\,dx\,dy \tag{12a}$$

$$e=a_1\bar{N}_{xx}-\frac{1}{L}\int_0^L\left[\alpha_1F_{,yy}+a_2F_{,xx}+a_3w_{,xx}\right.$$
$$\left.+a_4w_{,yy}-\frac{1}{2}w_{,x}(w_{,x}+2w^{\circ}_{,x})\right]_{y=0}dx \tag{12b}$$

Note that e measures the amount of end shortenting per unit of cylinder length, L. The associated boundary conditions are either kinematic or natural (but not both) except for the direction associated with the length of the cylinder (x), in which case the displacement component u is free, and the stress resultant N_{xx} must equal to the applied stress resultant $-\bar{N}_{xx}$. Thus at a boundary characterized by $x=0$ or $x=L$ the boundary conditions are

Either	or
in-plane	
$N_{xx}=F_{,yy}-\bar{N}_{xx}=-\bar{N}_{xx}$	$u=$ constant
$N_{xy}=0$	$v=0$
transverse	
$M_{xx}=0$	$w_{,x}=0$
$Q_x^*=0$	$w=0$

(13)

The expressions for the moment resultant M_{xx} and the effective transverse shear Q_x^* are

$$M_{xx}=\gamma_1w_{,xx}+\gamma_2w_{,yy}+\gamma_3(F_{,yy}-\bar{N}_{xx})+\gamma_4F_{,xx} \tag{14a}$$

$$Q_x^* = (F,_{yy} - \bar{N}_{xx})(w,_x + w^\circ,_x)$$
$$+ F,_{xy}(w,_y + w^\circ,_y) - M_{xx,x} - 2M_{xy,y} \tag{14b}$$

where

$$\gamma_1 = Dh_{11};\quad \gamma_2 = D\frac{\alpha_3}{2};\quad \gamma_3 = -\alpha_3;\quad \gamma_4 = -b_3$$

The general computer program is written for the following end conditions (*SSi, CCi, FFi*, $i=1,2,3,4$)

$$\left.\begin{array}{l} SS{:}\ w = M_{xx} = 0 \\ CC{:}\ w = w,_x = 0 \\ FF{:}\ Q_x^* = M_{xx} = 0 \end{array}\right\} \qquad \begin{array}{ll} 1. & F,_{xy} = F,_{yy} = 0 \\ 2. & F,_{xy} = 0;\ u = C \\ 3. & v = F,_{yy} = 0 \\ 4. & v = 0,\ u = C \end{array} \tag{15}$$

where C is a constant.

The conditions in u and v can be expressed in terms of w and F as in Ref. 14. For example *SS2* can be written as

$$0 = w = \gamma_1 w,_{xx} + \gamma_3 F,_{yy} + \gamma_4 F,_{xx} = F,_{xy}$$
$$= b_2 F,_{xxx} + b_3 w,_{xxx} + b_4 w,_{yyx} + \left(\frac{1}{R} + w^\circ,_{yy}\right) w,_x$$

In addition, the following conditions of symmetric and antisymmetric behavior, prevailing at the mid station ($x = L/2$), are incorporated into the computer program.

Symmetric conditions

$$w,_x = Q_x^* = F,_{xy} = u = 0 \tag{16a}$$

Antisymmetric condition

$$w = M_{xx} = v = F,_{yy} = 0 \tag{16b}$$

The problem, as formulated herein, is to find the limit point which represents the buckling load for the imperfect configuration. This implies solving the field equations, Eqs. (6) and (7), subject to the proper boundary conditions for a given imperfection and level of the applied load (small initially) $-\bar{N}_{xx}$ and thus obtain the corresponding amount of "unit end shortening," Eq. (12b). By plotting $\bar{N}_{xx}$ vs e one can obtain the limit point (theoretically).

III. Method of Solution

By employing the von Kármán-Donnell kinematic relations the field equations consist of two coupled, nonlinear, partial differential equations in terms of the transverse displacement w and the Airy stress function, F. The procedure employed herein for accomplishing a solution is basically similar to that of Ref. 13. The system of partial differential equations is reduced to a system of ordinary differential equations by using a separated solution (Fourier series) of the following form.[13,14]

$$w(x,y) = \sum_{i=0}^{K} W_i(x)\cos\frac{iny}{R} \tag{17}$$

$$F(x,y) = \sum_{i=0}^{2K} f_i(x)\cos\frac{iny}{R} \tag{18}$$

$$w^\circ(x,y) = \sum_{i=0}^{K} W_i^\circ(x)\cos\frac{iny}{R} \tag{19}$$

Note that $W_i^\circ(x)$ denotes the known coefficient of the ith component of the geometric imperfection, and n is the parameter associated with the number of full waves around the circumference.

By substituting Eq. (17) into Eq. (7), employing trigonometric identities of double Fourier series as in Ref. 19 involving products and the orthogonality of the trigonometric functions, the compatibility equation becomes

for $i=0$

$$f_0'' = \frac{1}{d_{11}}\left[-q_{11}W_0'' - W^\circ/R + \frac{n^2}{4R^2}\sum_{j=1}^{K} j^2(W_j + 2W_j^\circ)W_j\right] \tag{20a}$$

for $i = 1,2,\ldots 2K$

$$d_{11}f_i'''' - 2\left(\frac{in}{R}\right)^2 d_{12}f_i'' + \left(\frac{in}{R}\right)^4 d_{22}f_i$$
$$+\delta_i\left[q_{11}W_i'''' - 2\left(\frac{in}{R}\right)^2 q_{12}W_i'' + \left(\frac{in}{R}\right)^4 q_{22}W_i + W_i''/R\right]$$
$$-\frac{n^2}{4R^2}\sum_{j=0}^{K}\left\{\left[(i+j)^2\delta_{i+j}(W_{i+j} + 2W_{ij}^\circ)\right.\right.$$
$$\left.+(2-\eta_{j-i}^2)(i-j)^2\delta_{|i-j|}(W_{|i-j|} + 2W_{|i-j|}^\circ)\right]W_j''$$
$$[\delta_{i+j}(W_{i+j}'' + 2W_{i+j}^{\circ\prime\prime}) + (2-\eta_{j-i}^2)\delta_{|i-j|}(W_{|i-j|}''$$
$$+2W_{|i-j|}^{\circ\prime\prime})]j^2W_j + 2[(i+j)\delta_{i+j}(W_{i+j}' + 2W_{i+j}^{\circ\prime})$$
$$\left.-\eta_{i-j}|i-j|\delta_{|i-j|}(W_{|i-j|}' + 2W_{|i-j|}^{\circ\prime})]jW_j'\right\} = 0 \tag{20b}$$

where

$$\delta_\ell = \begin{cases} 0 & \ell > K \\ \\ 1 & \ell \le K \end{cases} \qquad \eta_\ell = \begin{cases} -1 & \ell < 0 \\ 0 & \ell = 0 \\ 1 & \ell > 0 \end{cases}$$

and

$$(\,)' = \frac{\mathrm{d}}{\mathrm{d}x}$$

Next, if Eqs. (17) are substituted into the equilibrium equation, Eq. (6), and the Galerkin procedure is employed (cos iny/R is the weighting function, $i=1,2,\ldots k$), the vanishing of the $(K+1)$ Galerkin integrals leads to the following system of $(k+1)$ ordinary differential equations:

for $i=0$

$$W_o''''[Dh_{11} + q_{11}^2/d_{11}] + W_o''[2q_{11}/R\cdot d_{11}] + W_o[1/R^2\cdot d_{11}]$$
$$+\bar{N}_{xx}(W_o'' + W_o^{\circ\prime\prime}) - \frac{n^2}{4R^2}\sum_{j=1}^{K} J^2\left\{\frac{q_{11}}{d_{11}}[(W_j + 2W_j^\circ)W_j''\right.$$
$$+(W_j'' + 2W_j^{\circ\prime\prime})W_j + 2(W_j' + 2W_j^{\circ\prime})W_j'] + \frac{1}{Rd_{11}}[(W_j$$
$$+2W_j^\circ)W_j] - 2[(W_j + W_j^\circ)f_j'' + (W_j'' + W_j^{\circ\prime\prime})f_j$$
$$\left.+2(W_j' + W_j^{\circ\prime})f_j']\right\} = 0 \tag{21a}$$

for $i = 1,2,\ldots,K$

$$D\left[h_{11}W_i'''' - 2\left(\frac{in}{R}\right)^2 h_{12}W_i'' + \left(\frac{in}{R}\right)^4 h_{22}W_i\right]$$
$$-\left[q_{11}f_i'''' - 2\left(\frac{in}{R}\right)^2 q_{12}f_i'' + \left(\frac{in}{R}\right)^4 q_{22}f_i + f_i''/R\right]$$

$$+\bar{N}_{xx}(W_i''+W_i^{\circ\prime\prime})_{,}-W_o''\left[\frac{q_{11}}{d_{11}}\left(\frac{in}{R}\right)^2\right](W_i+W_i^{\circ})-W_o\left[\frac{1}{Rd_{11}}\left(\frac{in}{R}\right)^2\right](W_i+W_i^{\circ})$$

$$+\frac{n^4}{4R^4}\frac{i^2}{d_{11}}(W_i+W_i^{\circ})\sum_{j=1}^{K}j^2(W_j+2W_j^{\circ})W_j+\frac{n^2}{2R^2}\sum_{j=1}^{2K}\Big\{[(i+j)^2\delta_{i+j}(W_{i+j}+W_{i+j}^{\circ})$$

$$+(2-\eta_{j-i}^2)(i-j)^2\delta_{|i-j|}(W_{|i-j|}+W_{|i-j|}^{\circ})]f_j''+[\delta_{i+j}(W_{i+j}''+W_{i+j}^{\circ\prime\prime})+(2-\eta_{j-i}^2)\delta_{|i-j|}(W_{|i-j|}''$$

$$+W_{|i-j|}^{\circ\prime\prime})]j^2f_j+2[(i+j)\delta_{i+j}(W_{i+j}'+W_{i+j}^{\circ\prime})-\eta_{i-j}|i-j|\delta_{|i-j|}(W_{|i-j|}'+W_{|i-j|}^{\circ\prime})]jf_j'\Big\}=0 \tag{21b}$$

For a given value of the applied load $\bar{N}_{xx}$ and imperfection, Eqs. (20) and (21) represent a system of $(3K+2)$ coupled nonlinear differential equations in $(3K+2)$ unknowns, f_i $i=0,1,2,\ldots 2K$ and W_i $i=0,1,2,\ldots,K$. These equations denote equilibrium and compatibility conditions. Similarly, the expressions for the total potential U_T average and shortening e_{AV}, and "unit end shortening" e become

$$U_T=\pi R\int_0^L\Big\langle\frac{1}{E_{xx_p}}\Big\{\frac{\beta_2}{d_{11}^2}\Big[-\frac{W_o}{R}-q_{11}W_o''+\frac{n^2}{4R^2}\sum_{i=1}^{K}i^2(W_i+2W_i^{\circ})W_i\Big]^2$$

$$+\frac{1}{2}\sum_{i=1}^{2K}\Big[\beta_1\Big(\frac{in}{R}\Big)^4f_i^2+\beta_2f_i''^2-\beta_3\Big(\frac{in}{R}\Big)^2f_i''f_i+\beta_4\Big(\frac{in}{R}\Big)^2f_i'^2\Big]\Big\}$$

$$+D\Big\{\alpha_2W_o''^2+\frac{1}{2}\sum_{i=1}^{K}\Big[\alpha_1\Big(\frac{in}{R}\Big)^4W_i^2+\alpha_2W_i''^2-\alpha_3\Big(\frac{in}{R}\Big)^2W_i''W_i+\alpha_4\Big(\frac{in}{R}\Big)^2W_i'^2\Big]\Big\}$$

$$-\frac{\bar{N}_{xx}\beta_3}{d_{11}E_{xxp}}\Big[-\frac{W_o}{R}-q_{11}W_o''+\frac{n^2}{4R^2}\sum_{i=1}^{K}i^2(W_i+2W_i^{\circ})W_i\Big]\Big\rangle dx+\frac{\beta_1\pi RL}{E_{xxp}}\bar{N}_{xx}^2-\bar{N}_{xx}2\pi R\,Le_{AV} \tag{22}$$

$$e_{AV}=a_1\bar{N}_{xx}+\frac{1}{L}\int_0^L\Big\{\frac{a_2}{d_{11}}\Big[\frac{W_o}{R}+q_{11}W_o''-\frac{n^2}{4R^2}\sum_{i=1}^{K}i^2(W_i+2W_i^{\circ})W_i\Big]$$

$$-a_3W_o''+\frac{1}{2}W_o'(W_o'+W_o^{\circ\prime})+\frac{1}{4}\sum_{i=1}^{K}W_i'(W_i'+W_i^{\circ\prime})\Big\}dx \tag{23a}$$

$$e=a_1\bar{N}_{xx}+\frac{1}{L}\int_0^L\Big\langle\frac{a_2}{d_{11}}\Big[\frac{W_o}{R}+q_{11}W_o''-\frac{n^2}{4R^2}\sum_{i=1}^{K}i^2(W_i+2W_i^{\circ})W_i\Big]+\sum_{i=1}^{2K}\Big[a_1\Big(\frac{in}{R}\Big)^2f_i-a_2f_i''\Big]$$

$$-a_3\sum_{i=0}^{K}W_i''+a_4\sum_{i=1}^{K}\Big(\frac{in}{R}\Big)^2W_i+\frac{1}{2}\Big[\sum_{i=0}^{K}W_i'\Big]\sum_{i=0}^{K}(W_i'+2W_i^{\circ\prime})\Big\rangle dx \tag{23b}$$

Finally, the appropriate boundary conditions are expressed in terms of W_i, W_i°, and f_i. Note that, because of the character of the nonlinear differential field equations, Eqs. (6) and (7), by setting $n=0$, one obtains the linearized version of equilibrium and compatibility. Furthermore, it is easily seen from Eq. (17) that $n=1$ includes the axisymmetric mode since the summation on i starts from zero. In addition, it is seen from the Fourier series representation of the imperfection that this expression is suitable for the case when the imperfection is of the same shape as the buckling mode as well as for any arbitrary symmetric (with respect to y) imperfection shape. In this latter case, in order to obtain a solution it is necessary to let $n=1$ (in the series representation for W°), and take K large enough for an accurate representation of the imperfection and for achieving a convergent solution.

The solution procedure employed is described below, in the following: A generalization of Newton's method,[20,21] applicable to differential equations, is employed to reduce the nonlinear field equations, Eqs. (20) and (21), and appropriate boundary conditions to a sequence of linear systems. In this method, the iteration equations are derived by assuming that the solution is achieved by a small correction to an approximate solution (initially taken as the linear solution). These small corrections are obtained through the solution of the linearized (with respect to the corrections) differential equations.

The linearized differential equations are written in matrix form as follows

Field equations

$$[A]\{Z''\}+[B]\{Z'\}+[C]\{Z\}=\{g\} \tag{24}$$

Boundary conditions

$$[\bar{A}]\{Z'\}+[\bar{C}]\{Z\}=\{\bar{g}\} \tag{25}$$

where $\{Z\}$ is the vector of the $6K+2$ unknowns.

$$\{Z\}=\{W_o,W_1,\ldots W_K,f_1,f_2\ldots f_{2K},\ W_o'',$$

$$W_1'',\ldots W_K'',\ f_1'',\ f_2'',\ldots f_{2K}''\} \tag{26}$$

Note that f_o has been eliminated in a manner similar to that of Refs. 13 and 14.

These ordinary differential equations are cast into the form of finite-difference equations, and the system of ordinary equations, Eqs. (24) and (25), are changed into a system of linear algebraic equations. The usual central difference formula is used at all mesh points, i.e.,

$$Z_\ell'=(Z_{\ell+1}-Z_{\ell-1})/2\Delta \qquad Z_\ell''=(Z_{\ell-1}-2Z_\ell+Z_{\ell+1})/\Delta^2 \tag{27}$$

Note that the second derivatives in W_i and f_i are taken as independent elements of the vector of the unknowns, therefore the second of Eq. (27) applies only to fourth derivatives of W_i and f_i. By using one fictitious point on each side of the cylinder ends one obtains a system of $(6K+2)\times(NP+2)$ difference equations (NP – number of mesh points).

When the load parameter is at a limit point a unique solution does not exist (the system becomes singular), and thus the solution does not converge. Therefore, the solution procedure goes as follows: first, the system of equations is solved for a small level of the applied load (say 20% of the classical buckling load), then a multiple of this solution is used for a small increase in the load parameter until the process fails to converge. The load level at which the solution fails to converge is taken to be the critical load. Note that, when approaching the limit load, if the increment in the load value is large enough so as to place the systems at equilibrium far beyond the limit point, the system, in some cases, does converge. In this case, since the interest is in the limit point value only, one can check the sign of the determinant of the coefficients of the unknown vector. If the sign changes, by taking a large increment in the load level, one must decrease the increment and proceed with the solution. Large increments are used in the procedure in order to save computer time. Because of the use of large increments and since, in some cases, the solution converged at both consecutive steps the criterion of the change in the determinant sign is employed to establish the existence of a critical point within the range of these consecutive steps. At each level of the load for which the system is solved, the value of the number of full circumferential waves is needed. Different values of n are used to obtain a solution, and the one that minimizes the total potential, Eq. (22), is taken as the correct one.[13] Numerical integration is used to find the total potential. The number of n values to be tried at every increment of the load is small since the circumferential mode does not vary significantly with small increases in the load, $\bar{N}_{xx}$. The end shortenings at each level of the applied load are also computed through numerical integration.

IV. Numerical Results and Discussion

The mathematical formulation and the method of solution for the buckling analysis of imperfect, thin, circular, stiffened cylindrical shells under uniform axial compression is presented in Secs. II and III. The methodology is demonstrated through a number of illustrative examples. Numerical solutions are obtained by employing the Georgia Tech high speed digital computer CDC-CYBER 70, Model 74-28. A general program is written (available to the reader by writing to the authors) which includes the following desirable features: a) it is applicable to stiffened (in either or both directions) geometries as well as unstiffened; b) accommodates all possible boundary conditions (*SS, CC, FF,* etc.), and it can easily be modified to accommodate elastic end restraints; c) the number of Fourier terms (K) can be as large as desired. The same holds true for the number of points (NP) in the finite-difference scheme; d) the geometric imperfection can be axisymmetric as well as an arbitrary symmetric (w.r.t.y) one. The program can easily be modified to include other destabilizing loading conditions such as pressure and torsion.

Although the program is highly dimensional because of the number of Fourier terms, number of points and number of required iterations, the solution is obtained with reasonable CPU time. For example, by using $K=1$ (one-term) and 65 points (536 unknowns) it requires four sec to complete one iteration; for the same but $K=2$ it requires 15 sec. For a convergent solution to be obtained at low levels of the applied load two iterations are sufficient. At load levels approaching the limit point six iterations are needed (convergence: percent difference $<10^{-4}$).

The numerical results for all the illustrative examples are presented in tabular form in Table 1. A number of these examples are taken from the open literature in order to check the present solution. In addition, new results are generated, and the discussion of both is given below. In this table, for each example considered, the buckling load (see columns of $\bar{N}_{xx_{cr}}$ and $\bar{N}_{xx_{cr}}/N_{xx_{cl}}$) is bracketed between two numbers (denoting the desired accuracy). The first number denotes the

Table 1 Final results for imperfect unstiffened and stiffened cylindrical shell

Example No.	$E = 10.5\cdot10^6$ $\nu = 0.3$ $R = 4.0$ Geometric parameters								Boundary Condition	linear buckling load perfect cylinder			Imperfection $w^0(x,y)$	Nonlinear limit point imperfect cylinder		
	L	t	$\frac{e_x}{t}$	$\frac{e_y}{t}$	$\bar{\lambda}_{xx}$	$\bar{\lambda}_{yy}$	$\bar{\rho}_{xx}$	$\bar{\rho}_{yy}$		$N_{x_{cl}}$	n	m		$N_{x_{cr}}$	$N_{x_{cr}}/N_{x_{cl}}$	n
1	4.	0.004	0	0	0	0	0	0	SS1	14.48*			$-0.5t\cos\frac{2\pi x}{L} + 0.05t\sin\frac{\pi x}{L}\cos\frac{ny}{R}$	12.50 ÷ 14.50	0.860 ÷ 1.000	12
2	4.	0.004	0	0	0	0	0	0	SS2	14.48*			$-0.5t\cos\frac{2\pi x}{L} + 0.05t\sin\frac{\pi x}{L}\cos\frac{ny}{R}$	14.00 ÷ 16.00	0.967 ÷ 1.105	15
3	4.	0.004	0	0	0	0	0	0	SS3	25.42			$-0.5t\cos\frac{2\pi x}{L} + 0.05t\sin\frac{\pi x}{L}\cos\frac{ny}{R}$	16.50 ÷ 16.56	0.649 ÷ 0.651	13
4	4.	0.004	0	0	0	0	0	0	CC1	25.42			$-0.5t\cos\frac{2\pi x}{L} + 0.05t\sin\frac{\pi x}{L}\cos\frac{ny}{R}$	16.88 ÷ 17.00	0.664 ÷ 0.669	13
5	4.	0.004	0	0	0	0	0	0	CC3	25.42			$-0.5t\cos\frac{2\pi x}{L} + 0.05t\sin\frac{\pi x}{L}\cos\frac{ny}{R}$	16.88 ÷ 17.00	0.664 ÷ 0.669	13
6	4.	0.04	-15.	0	1.82	0	1000.	0	SS3	123300.	0	1	$2t\sin\frac{\pi x}{L} + 0.2t\sin\frac{\pi x}{L}\cos\frac{ny}{R}$	73000. ÷ 78000.	0.592 ÷ 0.632	7
7	4.	0.04	-15.	0	1.82	0	1000.	0	SS3	123300.	0	1	$2t\sin\frac{\pi x}{L}\cos\frac{ny}{R}$	101450. ÷ 111450.	0.823 ÷ 0.903	1
8	8.125	0.04	-15.	0	1.82	0	1000.	0	SS3	58480.	5	1	$2t\sin\frac{\pi x}{L} + 0.2t\sin\frac{\pi x}{L}\cos\frac{ny}{R}$	19000. ÷ 20000.	0.325 ÷ 0.341	12
9	8.125	0.04	-15.	0	1.82	0	1000.	0	SS3	24810.	3	1	$2t\sin\frac{\pi x}{L} + 0.2t\sin\frac{\pi x}{L}\cos\frac{ny}{R}$	24000. ÷ 25000.	0.967 ÷ 1.007	3
10	8.125	0.04	0.	-3.	0.	0.455	0.	20.	SS3	3140.	2	13	$0.6t\sin\frac{\pi x}{L} + 0.06t\sin\frac{\pi x}{L}\cos\frac{ny}{R}$	1700. ÷ 1800.	0.541 ÷ 0.573	2
11	8.125	0.04	0.	3.	0.	0.455	0.	20.	SS3	2713.	5	11	$0.6t\sin\frac{\pi x}{L} + 0.06t\sin\frac{\pi x}{L}\cos\frac{ny}{R}$	1600. ÷ 1725.	0.589 ÷ 0.635	2
12	4.	0.04	-6.	-3.	0.91	0.455	100.	20.	SS3	35220.	4	1	$0.5t\sin\frac{\pi x}{L} + 0.05t\sin\frac{\pi x}{L}\cos\frac{ny}{R}$	26500. ÷ 28000.	0.752 ÷ 0.795	4
13	4.	0.04	-6.	-3.	0.91	0.455	100.	20.	SS3	35220.	4	1	$0.5t\sin\frac{\pi x}{L}\cos\frac{ny}{R}$	25000. ÷ 26500.	0.710 ÷ 0.752	4
14	4.	0.04	-6.	-3.	0.91	0.455	100.	20.	SS3	35220.	4	1	$1.0t\sin\frac{\pi x}{L}\cos\frac{ny}{R}$	20500. ÷ 22000.	0.582 ÷ 0.625	4
15	4.	0.04	-6.	-3.	0.91	0.455	100.	20.	SS3	35220.	4	1	$2.0t\sin\frac{\pi x}{L}\cos\frac{ny}{R}$	16000. ÷ 16750.	0.454 ÷ 0.476	4
16	4.	0.04	-6.	-3.	0.91	0.455	100.	20.	SS3	35220.	4	1	$4.0t\sin\frac{\pi x}{L}\cos\frac{ny}{R}$	13000. ÷ 13500.	0.369 ÷ 0.383	4
17	4.	0.04	6.	3.	0.91	0.455	100.	20.	SS3	19790.	4	1	$0.5t\sin\frac{\pi x}{L} + 0.05t\sin\frac{\pi x}{L}\cos\frac{ny}{R}$	17000. ÷ 17500.	0.859 ÷ 0.884	4
18	4.	0.04	6.	3.	0.91	0.455	100.	20.	SS3	19790.	4	1	$0.5t\sin\frac{\pi x}{L}\cos\frac{ny}{R}$	17000. ÷ 17500.	0.859 ÷ 0.884	4
19	4.	0.04	6.	3.	0.91	0.455	100.	20.	SS3	19790.	4	1	$1.0t\sin\frac{\pi x}{L}\cos\frac{ny}{R}$	15250. ÷ 15630.	0.771 ÷ 0.790	4
20	4.	0.04	6.	3.	0.91	0.455	100.	20.	SS3	19790.	4	1	$2.0t\sin\frac{\pi x}{L}\cos\frac{ny}{R}$	13750. ÷ 14500.	0.695 ÷ 0.733	4
21	4.	0.04	6.	3.	0.91	0.455	100.	20.	SS3	19790.	4	1	$4.0t\sin\frac{\pi x}{L}\cos\frac{ny}{R}$	11200. ÷ 11400.	0.566 ÷ 0.576	3

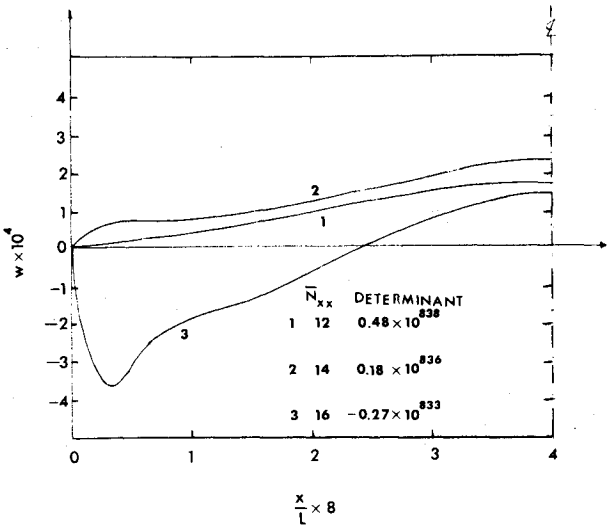

Fig. 2 Radial displacement along $y=0$ (Example 2).

highest level of the load for which a convergent solution is obtained and the second number a level higher than the limit point (according to criterion discussed herein). Note that the difference between the two numbers can be made as small as one wishes by taking smaller increments in the applied load. In all examples, the imperfection is taken to be symmetric with respect to $x=L/2$, and therefore the response is taken to be symmetric. Thus only half of the cylinder is analyzed by employing the appropriate symmetric conditions at $x=L/2$. The examples can broadly be classified in one of the following four categories: a) unstiffened (Examples 1-5); b) stringer-stiffened (Examples 6-9); c) ring-stiffened (Examples 10 and 11); and d) ring- and stringer-stiffened (Examples 12-21). In each of the four categories, at least one case is calculated for two different truncated Fourier series ($K=1$ and $K=2$) and for two different number of points ($NP=35$ and $NP=65$) in order to check the effect of these two parameters on the convergence of the solution.

The linear buckling classical loads for all geometries with *SS*3 boundary conditions are computed by employing the program used in Ref. 18. For *SS*1 and *SS*2 boundary conditions (examples 1 and 2), $N_{x_{cl}}$ is estimated to be 0.57 times the *SS*3 classical value. These numbers are taken from Ref. 13. Finally, for *CC*1 and *CC*3 (examples 4 and 5) $N_{x_{cl}}$ is taken to be the same as the *SS*3 classical value.[23]

Table 2 Computations for estimating n and $\bar{N}_{xx_{cr}}$ (Example 14)

$\bar{N}_{xx}$	$\frac{\bar{N}_{xx}}{\bar{N}_{x_{cl}}}$	n	k	Points NP	Total Potential	"end shortening"	No. of Iterations	CPU TIME (SEC)
19000	0.54	3	1	35	-10777.	0.021870	3	9
22000	0.62	3	1	35	-14499.	0.025424	4	11
23500	0.67	3	1	35	-16590.	0.027394	4	12
25000	0.71	3	1	35	over limit point			
13000	0.37	4	1	35	- 5028.	0.015124	3	9
16000	0.45	4	1	35	- 7628.	0.018620	3	9
19000	0.54	4	1	35	-10785.	0.022161	4	11
22000	0.62	4	1	35	-14534.	0.026189	6	20
22750	0.65	4	1	35	over limit point			
19000	0.54	4	1	65	-10784.	0.022160	4	19
22000	0.62	4	1	65	-14534.	0.026188	6	33
22750	0.65	4	1	65	over limit point			
19000	0.54	4	2	65	-10789.	0.022232	4	70
20500	0.58	4	2	65	-12590.	0.024197	5	90
22000	0.62	4	2	65	over limit point			
19000	0.54	5	1	35	-10745.	0.022248	4	11
22000	0.62	5	1	35	-14443.	0.025847	4	11
22750	0.65	5	1	35	-15459.	0.026813	5	15
23500	0.67	5	1	35	over limit point			
22000	0.62	6	1	35	-14362.	0.025764	4	11
22000	0.62	7	1	35	-14318.	0.025762	3	9
22000	0.62	12	1	35	-14267.	0.025758	2	7

a) *Unstiffened (Examples 1-5)*. This geometry is taken from Ref. 16. Only Example 5 is reported in Ref. 16, and the results are in very good agreement. Examples 1,2,3, and 4 are considered in order to assess the effect of boundary conditions for this type of an imperfection (see Table 1). It is seen from the results that the effect of in-plane boundary conditions is significant for the simply supported case and insignificant for the clamped case. In Example 2, because of the $u=c$ in-plane boundary condition, the criterion used for finding $\bar{N}_{xx_{cr}}$ is that the determinant (see Section 3) goes to zero. It can be seen from Fig. 2 that as the sign of the

Table 3 Effect of number of Fourier terms and grid points on the response amplitudes

$$w^{\circ}(x,y)=\delta_2 \sin\frac{\pi x}{L}\cos\frac{ny}{R}$$

δ_2/t	K	No. of Points	Examples	$\frac{N_{x_{cr}}}{N_{x_{cl}}}$	w_0	w_1	w_2	f_1	f_2	f_3	f_4
1.0	1	35	14	0.539	0.009172	0.052284	--	2246.40	-77.13	--	--
1.0	1	65		0.539	0.009167	0.052270	--	2245.88	-77.12	--	--
1.0	2	65		0.539	0.009894	0.055149	0.0035991	2306.74	-39.86	-4.55	-0.45
1.0	1	35		0.625	0.024436	0.096853	--	3976.12	-191.04	--	--
1.0	1	65		0.625	0.024401	0.096768	--	3973.14	-190.83	--	--
1.0	2	65		0.582	0.015810	0.074324	0.0058296	3018.11	-60.28	-8.86	-0.12
1.0	2	65		0.625	over limit point						
1.0	1	65		0.646	over limit point						
2.0	1	35	15	0.454	0.026022	0.086314	--	3405.72	-236.92	--	--
2.0	1	65		0.454	0.026005	0.086281	--	3404.66	-236.86	--	--
2.0	2	65		0.454	0.034229	0.105602	0.0114593	3699.64	-194.83	-28.22	-0.4501
2.0	1	35		0.497	over limit point						
2.0	1	65		0.497	over limit point						
2.0	2	65		0.476	over limit point						
4.0	1	35	16	0.369	0.113547	0.201740	--	4794.98	-1166.29	--	--
4.0	2	65		0.369	0.132664	0.230965	0.21715	3549.32	-1342.51	-109.53	-1.37
4.0	1	35		0.383	over limit point						
4.0	2	65		0.383	over limit point						
1.0	1	35	19	0.771	0.036821	0.164462	--	1483.81	-447.37	--	--
1.0	2	65		0.771	0.036716	0.164500	0.002221	1409.59	-461.42	-5.957	-0.0159
1.0	1	35		0.790	over limit point						
1.0	2	65		0.790	over limit point						

→ 3% Difference

→ 4% Difference

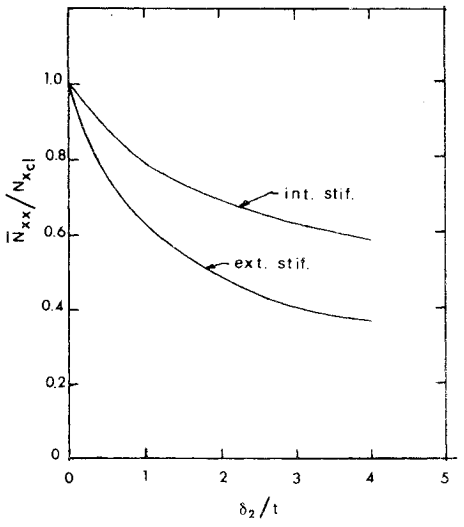

Fig. 3 Effect of amplitude of symmetric imperfection on the critical load (Examples 13-16 and 18-21).

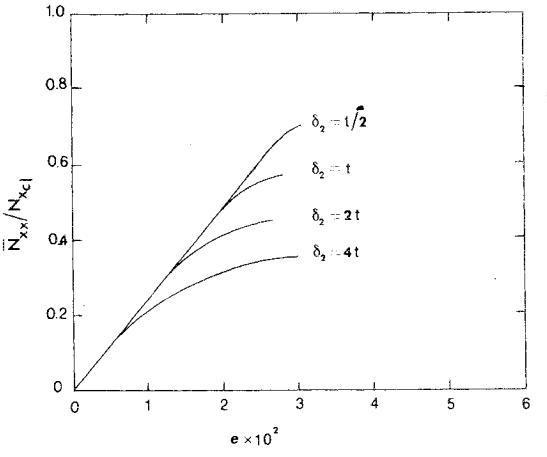

Fig. 4 Load vs "unit end shortening" (Examples 13-15).

determinant changes the radial mode of deformation changes. The calculations for this case are based on $K=1$ and 65 grid points in the axial direction (for half the cylinder length).

b) *Stringer-stiffened (Examples 6-9)*. The geometry for these examples is taken from Ref. 9 and referred to, in it, as heavy stringers. The present results are in very good agreement with those of Ref. 9. Examples 6 and 7 correspond to $Z=95.4$ with external stringers, and the imperfection shape is virtually axisymmetric in Example 6, and symmetric in Example 7. The axisymmetric imperfection yields greater reduction than the symmetric one. Note that, for this case, the perfect geometry buckles axisymmetrically. Examples 8 and 9 correspond to $Z=394$ with external and internal stringers, respectively, and an imperfection which is primarily axisymmetric. From these examples one can conclude (as in Ref. 9) that imperfection sensitivity is greatly affected by the curvature parameter Z, and that externally stiffened configurations are much more sensitive to geometric imperfection than internally stiffened ones. These cases are analyzed with 35 and 65 grid points in the axial direction for half the cylinder length. From these computations one can see (for a typical case, see Tables 2 and 3), that the critical load and the response (w,F) for each n are almost the same regardless of the number of points.

c) *Ring-stiffened (Examples 10 and 11)*. This geometry is also taken from Ref. 9, and it corresponds to light ring-stiffened cylinders with $Z=394$ and external and internal positioning of the rings respectively. Although the numerical results of the present analysis are in good agreement with those of Ref. 9, the conclusion concerning the effect of ring positioning on the sensitivity is reversed. According to the present results internal rings make the overall configuration more sensitive than external rings.

d) *Ring- and stringer-stiffened (Examples 12-21)*. These examples are chosen to demonstrate the methology for ring- and stringer-stiffened configurations. In addition, the geometries are chosen in such a way that some comparison can be given with stiffened configurations of the only stringer- or ring-stiffened type. These examples correspond to a geometry for which $Z=95.4$, $(e_x/t)=\pm 6$, $(e_y/t)=\pm 3$, $\bar{\lambda}_{xx}=0.91, \bar{\lambda}_{yy}=0.455$, $\bar{\rho}_x=100$, and $\bar{\rho}_y=20$ (see Table 1). The imperfection shape is taken to be similar to the buckling mode, and the imperfection amplitude is varied from half to four times the thickness of the skin. The reader is reminded that the analysis is based on the smeared technique. According to Ref. 9 this configuration without rings is highly sensitive to geometric imperfections when the stringers are positioned on the outside and virtually insensitive for inside positioning of the stringers. The present results (see Table 1) indicate that with the presence of rings the sensitivity is reduced for external stiffeners and aggravated (increased) for internal stiffeners. Examples 12-16 correspond to external stiffening, while examples 17-21 correspond to internal stiffening. The configuration is checked for a primarily axisymmetric imperfection (examples 12 and 17) as well as symmetric imperfections (remaining examples). The effect of the imperfection amplitude is checked for symmetric imperfections and both external and internal stiffening. This effect is shown graphically on Fig. 3. Figure 4 shows the plots of load versus "unit end shortening" for three amplitudes of the symmetric imperfection and external stiffeners. Table 2, which corresponds to example 14 but is typical for all examples considered, depicts in tabular form the computational procedure required to arrive at the final results shown in Table 1. From this table one can see that the minimum total potential corresponds to $n=4$. For this n value, all results are the same for $NP=35$, and $NP=65$. In addition, when $K=1$ and $K=2$, the critical load differs by 4% or less. Table 3 presents a comparison of response (radial displacement and stress function amplutides), and critical loads for different K values (number of Fourier terms), and two different values of NP (number of grid points).

Conclusions

A methodology for the buckling analysis of imperfect, thin, curcular cylindrical, stiffened shells under uniform axial compression and for various end conditions is presented and demonstrated through a number of examples. On the basis of the results reported herein very few, if any, general conclusions can be drawn. Among these one may list the following:

1) It seems that the imperfection sensitivity of generally stiffened configurations strongly depends on the curvature parameter.

2) From the examples considered it appears that configurations with external stiffening are more imperfection sensitive than configurations with internal stiffening.

3) The few examples considered seem to support the contention that the most severe shape of imperfection is that which resembles the buckling mode.

4) The curve that demonstrates the effect of the imperfection amplitude on the critical load seems to be approaching a finite asymptote (see Fig. 3).

5) The presence of both stringers and rings in a configuration alters the conclusions regarding the effects of positioning of the stiffeners of the curvature parameter on the imperfection sensitivity of a configuration with either strings or rings only. The limited generated data suggests a nonlinear coupling of the individual effects.

6) In general one should not expect the wave number, corresponding to the limit point for an imperfect cylinder, to

be the same as the one predicted by the linear analysis of the corresponding perfect geometry. This difference, though, seems to be minimized when the configuration is stiffened in both direction (see Table 1; Examples 12-21).

Acknowledgment

Research sponsored by the Air Force Office of Scientific Research, Air Force Systems Command, USAF, and AFOSR Grant No. 74-2655.

References

[1]Von Karman, T. H. and Tsien, H. S., "The Buckling of Thin Cylindrical Sheels under Axial Compression," *Journal of the Aeronautical Sciences*, Vol. 8, Aug. 1941, pp. 303-312.

[2]Micheelsen, H. F., "The Behavior of Thin Cylindrical Shells after Buckling under Axial Compression," *Journal of the Aeronautical Sciences*, Vol. 15, Nov. 1948, pp. 738-744.

[3]Kempner, J., "Postbuckling Behavior of Axially Compressed Circular Cylindrical Shells," *Journal of the Aeronautical Sciences*, Vol. 17, May 1954, pp. 329-342.

[4]Almroth, B. O., "Postbuckling Behavior of Axially Compressed Circular Cylinder," *AIAA Journal*, Vol. 1, March 1963, pp. 630-633.

[5]Hoff, N. J., Madson, W. R., and Mayers, J., "The Postbuckling Equilibrium of Axially Compressed Circular Cylindrical Shells," *AIAA Journal*, Vol. 4, Jan. 1966, pp. 126-133.

[6]Madson, W. A. and Hoff, N. J., "The Snap-through and Postbuckling Equilibrium Behavior of Circular Cylindrical Shells under Axial Load," SUDAER N. 227, Stanford University, Stanford, Calif., Aug. 1965.

[7]Koiter, W. T., "On the Nonlinear Theory of Thin Elastic Shells," *Koninklizke Nederlandse Akademic Van Weleschappen*, Vol. 69, No. 1, Jan. 1966, pp. 1-54.

[8]Koiter, W. T., "On the Stability of Elastic Equilibrium," Thesis, Polytechnic Institute of Delft, H. J. Paris, Amsterdam, 1945 (in Dutch).

[9]Hutchinson, J. W., and Amazigo, J. C., "Imperfection Sensitivity of Eccentrically Stiffened Cylindrical Shells," *AIAA Journal*, Vol. 5, March 1967, pp. 392-401.

[10]Hoff, N. J., "The Perplexing Behavior of Thin Circular Cylindrical Shells in Axial Compression," *Israel Journal of Technology*, Vol. 4, No. 1, Feb. 1966, pp. 1-28.

[11]Hutchinson, J. W. and Koiter, W. T., "Posbuckling Theory," *Applied Mechanics Reviews*, Vol. 12, Sept. 1970, pp. 1353-1366.

[12]Thielemann, W. F. and Esslinger, M. E., "On the Postbuckling Behavior of Thin Walled Axially Compressed Circular Cylinder of Finite Length," *Proceedings of the 70th Anniversary Symposium on the Theory of Shells to Honor Lloyd Hamilton Donnel*, edited by D. Muster, Univ. of Houston, Houston, Texas, 1967, pp. 433-479.

[13a]Narasimhan, K. Y., and Hoff, N. J., "Snapping of Imperfect Thin-Walled Circular Cylindrical Shells of Finite Length," *Journal of Applied Mechanics*, Vol. 93, No. 1, March 1971, pp. 162-171.

[13b]Narasimhan, K. Y. and Hoff, N. J., "Calculation of the Load Carrying Capacity of Initially Slightly Imperfect Thin Walled Circular Cylindrical Shells of Finite Length," SUDAER No. 329, Stanford University, Stanford, Calif., Dec. 1967.

[14]Keller, H., *Numerical Method for Two Point Boundary-Value Problems*, Blaisdell Publishing Co., Waltham, Mass., 1968.

[15]Arborx, J and Sechler, E. E., "On the Buckling of Axially Compressed Imperfect Cylindrical Shells," *Journal of Applied Mechanics*, Vol. 41, No. 3, Transactions of the ASME, Vol. 96, Series E, Sept. 1974, pp. 737-743.

[16]Ball, R. E. and Ryan, B. A., "Computer Analysis of Buckling of Imperfect Shells," *Journal of Structures Div.*, ASCE, Vol. 99, (ST 10), Oct. 1973, pp. 2098-2108.

[17]Donnell, L. H., "A New Theory for the Buckling of Thin Cylinder Under Axial Compression and Bending," *Transactions of the ASME*, Vol. 56, No. 11, Nov. 1934, p. 795.

[18]Simitses, G. J. and Ungbhakhorn, V., "Minimum Weight Design of Stiffened Cylinders under Axial Compression," *AIAA Journal*, Vol. 13, June 1975, pp. 750-755.

[19]Sheiman, I. and Tene Y., "Buckling in Segmented Shells of Revolution Subjected to Symmetric and Antisymmetric Loads," *AIAA Journal*, Vol. 12, Jan. 1974, pp. 15-20.

[20]Thurston, G. A., "Newton's Method Applied to Problems in Nonlinear Mechanics," *Journal of Applied Mechanics*, Vol. 32, No. 2, June 1965, pp. 383-388.

[21]Thurston, G. A. and Freeland, M. A., "Buckling Imperfect Cylinders under Axial Compression," NASA CR-541, July 1966.

[22]Tene, Y., Epstein, M., and Sheinman, I., "A Generalization of Potter's Method," *Computer Structures*, Vol. 4, Dec. 1974, pp. 1099-1103.

[23]Hoff, N. H., and Soong T. C., "Buckling of Circular Cylindrical Shells in Axial Compression," SUDAER No. 204, Stanford University, Stanford, California, Aug. 1964.